Research on Engineering Structures & Materials
www.jresm.org

*Research Article*

# Impact of the rigid piles on the dynamic response of the soil-inclusions-mattress-slab system under seismic excitations

Oussama Benmerabet [*,1,a], Salah Messioud [1,b], Rania Beghila [2,c], Daniel Dias [3,d]

[1]*LGCE Laboratory, Faculty of Sciences and Technology, University of Jijel, Algeria*
[2]*LEEGO Laboratory, Faculty of Civil Engineering, University of Sciences and Technology Houari Boumediene (USTHB), Algeria*
[3]*3SR Laboratory/Polytech, Grenoble Alpes University, France*

**Article Info**

***Article History:***

Received 24 Mar 2025
Accepted 02 June 2025

***Keywords:***

Code-Aster;
Numerical modeling;
Rigid inclusions;
Seismic loading;
Soil-structure interaction

**Abstract**

This paper presents a numerical model of the dynamic response of the soil-inclusions-mattress-slab system under seismic loading, with a particular focus on analyzing the influence of inclusions on the reinforcement system. Three-dimensional finite element numerical models with absorbing boundaries based on the direct method are utilized for this study using Code-Aster software. The analysis accounts for two different types of soil behavior: non-linear elastic and elasto-plastic. Six models were simulated in this study, each varying in the number of inclusions, to investigate how the number of inclusions impacts the overall behavior of the system and the variation in internal stresses and horizontal displacements within each inclusion. The objective of this numerical model is to study the influence of the number of inclusions on the dynamic response of a reinforcement system, for both elastic and elasto-plastic behaviors, using the Mohr-Coulomb criterion. The study's findings reveal that an increase in the number of inclusions leads to reduced stresses and displacements within the inclusions. Moreover, inclusions positioned closer to the perimeter of the inclusion network, farther from the point of loading application, experience lower stress levels and are less prone to displacements compared to those located at the network's center. Regarding the impact of considering elastic or elasto-plastic behavior, the results of elasto-plastic calculation are compared with those of non-linear elastic calculation. The results indicate that assuming elasto-plastic behavior in calculations results in decreased internal stresses rather than an increase in displacement.



## 1. Introduction

Various compressible soils are commonly employed in civil engineering projects. The utilization of soft soil improvement techniques becomes essential as regions with suitable soil for constructing highways, railroads, and industrial networks become scarce. When the quality of these soils is inadequate, engineers opt for deep foundations to reach soil layers that offer better support. Addressing surface settlement issues can be achieved through the use of Rigid Inclusions (RIs). Additionally, this method is both efficient and eliminates the necessity for substituting soft soil [1-4].

The utilization of rigid inclusions as a soil reinforcement technique offers an intriguing alternative to conventional methods, such as pre-loading or vertical drainage. It addresses environmental concerns while optimizing costs and construction timelines. This approach can significantly

*Corresponding author: oussama.benmerabet@univ-jijel.dz
[a]orcid.org/0000-0003-3731-5121; [b]orcid.org/0000-0003-0368-9854; [c]orcid.org/0009-0006-8486-6531; [d]orcid.org/0000-0003-2238-7827
DOI: http://dx.doi.org/10.17515/resm2025-778st0324rs

enhance the initial bearing capacity of the soil and reduce foundation settlements under applied loads, thereby enhancing stability [5-8].

The process of reinforcement involves creating a composite foundation where the loads are distributed between the soil and the rigid inclusions. Compressible soil is strengthened by introducing a network of inclusions that traverse it, supported by a more rigid layer, along with a granular mattress positioned between the reinforced soil and the surface structure. Specifically, soil reinforcement encompasses various techniques aimed at incorporating vertical elements into the soil to improve its load-bearing capacity under static or dynamic loads, such as those exerted by embankments or surface foundations. It is also employed to counteract the pressure of soil in the case of support or stabilization works on natural slopes [2, 9, 10].

Structures supported by soils reinforced with rigid inclusions may encounter various types of loading, both static and dynamic. To gain a comprehensive understanding of the dynamic response of structures subjected to seismic loading, it is crucial to study the dynamic behavior of groups of rigid inclusions. In the past four decades, there has been a notable surge in the analysis of foundation behavior under dynamic stresses. Analytical methods have greatly benefited from the stringent safety requirements imposed on the design of particular types of structures [11].

The use of deep foundations in seismic regions raises several important questions, including the role of the mattress in altering the free-field response of the ground (amplification) and in distributing loads within the inclusions. In the case of rigid inclusions, direct contact between the structure and the inclusions is avoided because the distribution mattress acts as an intermediary [5]. The granular mattress, often referred to as the Load Transfer Platform (LTP), serves the purpose of transmitting the load applied at the surface to the heads of the inclusions through mechanisms such as the curved effect. This process is influenced by differential settlement between the inclusions and the compressible soil, as well as the friction within the granular soil. The mattress can be constructed using various materials, whether untreated or treated, such as lime or cement [12, 13]. This technique involves the integration of a grid of vertical rigid inclusions with a supporting layer and an intermediate mattress to create a system for distributing both vertical and horizontal stresses. The primary objective of this assembly is to facilitate the transfer of vertical loads from the surface to the supporting layer, consequently mitigating stresses on the compressible soil and minimizing settlement of the structure [14-16].

The analysis of how rigid inclusions respond to seismic forces requires solving a soil-structure interaction (SSI) problem that accounts for the unique components of the reinforcement system provided by the rigid inclusions. These components include the soil, the inclusions themselves, the distribution mattress, and the structure. This challenge is characterized by its three-dimensional and non-linear nature. SSI falls within the realm of applied mechanics, focusing on the development and examination of practical and theoretical methodologies for assessing structures subjected to dynamic loads while considering the behavior of both the soil and the structure [17-19].

In essence, SSI investigates how the ground's motion changes during an earthquake or under dynamic loads due to the presence of a structure. The significance of this interaction varies depending on factors such as the soil's properties, the structure's characteristics, and its foundation type. These structures encompass a wide range of applications, including nuclear power plants, power facilities, liquefied natural gas tanks (LNG), dams, and more [8, 20, 21]. In the early stages of research on soil-structure interaction (SSI), there was limited emphasis on analyzing high-rise buildings from an SSI perspective, primarily because they were classified as lightweight structures. Traditionally, seismic response evaluations of these structures were carried out without considering the influence of SSI. However, this perspective has evolved significantly due to damage assessment reports following recent devastating earthquakes, highlighting the substantial impact of SSI effects [8, 22-24].

Taking into account the influence of soil-structure interaction (SSI), the soil domain is typically characterized by an elasto-plastic behavior governed by the Mohr-Coulomb yield criterion. Addressing this complex issue requires a comprehensive investigation, including aspects such as defining seismic hazards and resulting ground motion, studying soil behavior under dynamic and cyclic loading, and assessing the response of open field soil and structures to seismic loads [19, 25].

In general, various approaches have been proposed for analyzing SSI and can be categorized into different methods: direct methods, substructure methods, and hybrid methods. Each of these methods corresponds to a specific representation of the soil-structure model [26-30].

The direct method, also known as global methods, is often considered the most rigorous approach for addressing SSI, especially in cases involving complex structural geometries and non-linear soil modeling. This method involves directly solving the motion equation of the soil-structure system. It simultaneously accounts for the behaviors and contact conditions of soil, foundation, and structural elements within the same analysis. These methods allow for the consideration of critical factors in SSI, including soil heterogeneity, the presence of water, the non-linear behavior of geomaterials, and soil-structure contact conditions [26, 31, 32].

This paper explores the dynamic response of soil-rigid inclusions-mattress-slab systems subjected to seismic loading. The investigation employs three-dimensional finite element numerical models with absorbing boundaries, utilizing the direct method. This work is oriented towards the qualification and quantification of solicitations and displacements in soil-piles-mattress-slab systems subjected to seismic loading, in order to study the effectiveness of soil reinforcement systems (soil-piles-mattress- slab), and to study the impact of the number of inclusions on the dynamic response of the system, for both elastic and elasto-plastic with Mohr-Coulomb criterion behaviors. The results of elasto-plastic calculation are compared with those of non-linear elastic calculation.

## 2. Numerical Study of The Soil–Pile–Mattress–Slab Interaction

### 2.1 Finite Element Method (FEM)

SSI analysis is categorized based on the method of analysis, treatment of the superstructure and soil, and the approach to handling interactions using various techniques. In SSI investigations, the primary computational techniques for discretizing the soil domain include the Finite-Element Method (FEM), Finite-Difference Method (FDM), and Boundary-Element Method (BEM). Among these, FEM has proven to be the most suitable approach for modeling and analyzing complex problems like SSI, covering a wide range of physical scenarios. It is a method used to approximate solutions within a spatial domain, allowing for the calculation of fields (scalars, vectors, tensors) that satisfy specific equations and imposed conditions. The versatility of this method has led to its increasing use in studying a diverse array of cases [32-37].

The Finite Element Method (FEM) is grounded in a straightforward concept: it involves dividing a complex shape into numerous elementary subdomains with simple geometric forms, known as finite elements, and connecting them at specific points referred to as "nodes." The process begins by constructing a mesh that incorporates the various elements of the system. Subsequently, material behavior laws for each component are selected, and finally, the problem is solved through numerical methods [27, 38].

The rigid inclusion reinforcement system is composed of a mattress, which is further covered by a reinforced concrete slab and subjected to seismic loading. In this study, a 3D numerical modeling approach using the Finite Element Method (FEM) with absorbing boundaries is employed. Initially, the analysis considers the non-linear elastic behavior of the soil, followed by the consideration of elasto-plastic behavior. The modeling includes the representation of inclusions using bar elements, the slab using shell elements, and the soil and mattress using volume elements. Furthermore, the analysis accounts for complex conditions involving balance compatibility, material behavior, and boundary conditions [23, 39, 40].

Absorbing boundaries are an essential addition to this method because the numerical model cannot encompass the entire domain. To simulate the semi-infinite elastic space, Free-field boundaries are attributed to the vertical faces and to the bottom face of the numerical model. Paraxial elements are assigned to the free boundaries to answer soil-structure interaction problems and avoid wave reflection to satisfy the Sommerfeld conditions. These boundaries should be positioned at a significant distance from the structure to reduce computation time and prevent wave reflections at the soil-structure interface during the analysis [40-42]. The geometric characteristics of the model

were determined using a parametric study to ensure the correct functioning of the absorbing boundaries.

## 2.2 Model Characteristics

A parametric study was conducted to determine the geometric properties of the model, ensuring the proper functioning of the absorbing boundaries. The maximum wavelength dictates the dimensions of the model as well as the element sizes. The soil volume consists of two layers with distinct characteristics. The base layer is a substratum measuring 35×35×5 meters, while the layer above is a 35×35×10 meters volume of compressible soil with unfavorable characteristics. To address the poor characteristics of the upper layer, it is reinforced with rigid concrete inclusions. These inclusions have a length of 10 meters, a circular section with a diameter of d = 0.3 meters, and are spaced at intervals of S = 3 meters. On top of the compressible soil layer, there is a load transfer mattress measuring 0.6 meters in thickness, which is further covered by a reinforced concrete slab also measuring 0.6 meters in thickness.

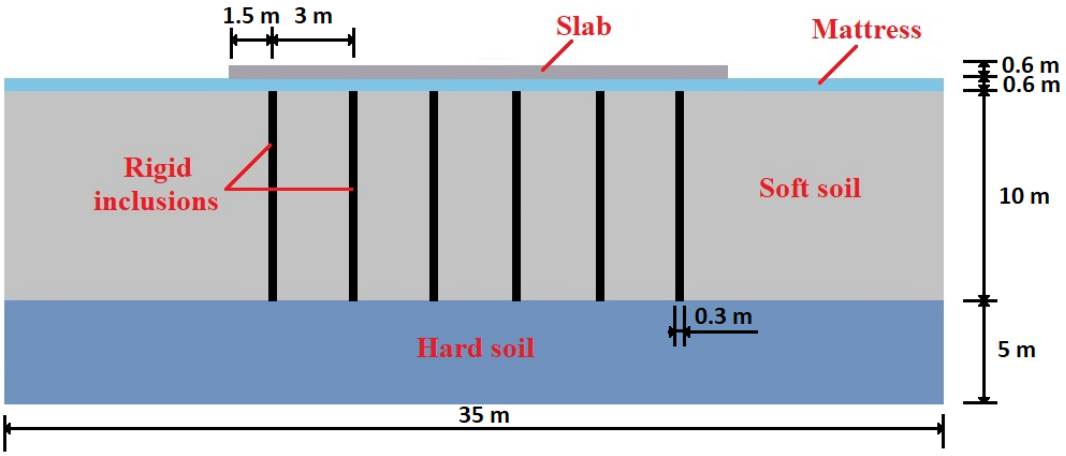


(a)

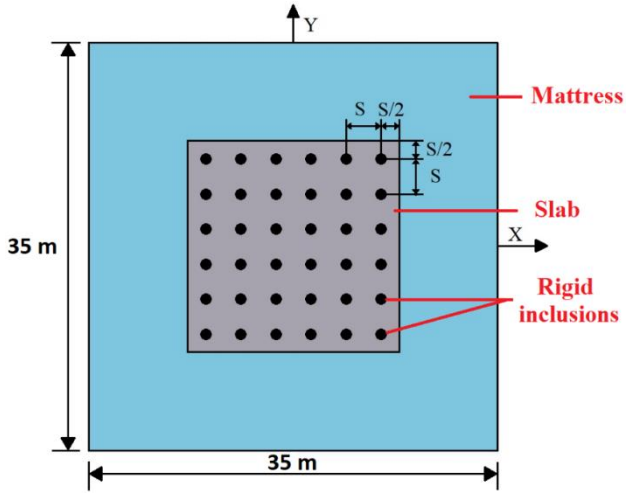


(b)

Fig. 1. Schematic representation of the analyzed systems: (a) Cross section of system. (b) Plan view and location of the vertical inclusions

At the bottom of the hard soil layer, which serves as the base for the systems under investigation, the seismic force is applied. Table 1 provides the mechanical characteristics of the soil layers and the transfer mattress. The choice of these properties was informed by the works of [43-45]. The damping ratio, angle of friction, angle of dilatancy, and cohesion are used in the calculation, which accounts for the elasto-plastic behavior of soils. Wave damping in soil generally results from its viscous properties, friction, and the development of plasticity. A linear elastic model for soil layers

does not explicitly represent viscosity. Therefore, 5% Rayleigh damping is introduced for all interactig elements.

Table 1. Geo-mechanical parameters of the model elements.

| Parameter / Element | Elastic modulus E (MPa) | Poisson ratio υ | Density ρ (kg/m³) | Cohesion, c (Pa) | Damping ratio ζ | Angle of friction, θ (°) | Angle of dilatancy, ψ(°) |
|---|---|---|---|---|---|---|---|
| Rigid inclusion | 25000 | 0.25 | 2500 | - | - | - | - |
| Slab | 25000 | 0.25 | 2500 | - | - | - | - |
| Mattress | 50 | 0.4 | 2000 | 50000 | 0.5 | 25 | 10 |
| Soft soil | 10 | 0.4 | 1800 | 5000 | 0.5 | 25 | 10 |
| Hard soil | 100 | 0.4 | 2200 | 5000 | 0.5 | 25 | 10 |

## 2.3 Methods of Analysis and Evaluation

Code-Aster is free Finite Element Analysis (FEA) software for numerical simulation in structural mechanics. This software provides around 400 different types of finite elements for discretizing solids and a large range of solvents, all of which have been subject to a rigorous and continuous verification and validation process. Developed since 1989 by EDF (Électricité De France Company) for the study of structure behavior by finite elements, it supports static, dynamic, and vibratory analysis of mechanically charged structures, as well as modal analysis. [45-47].

A study utilizing Code-Aster necessitates the implementation of a finite element mesh in conjunction with a command file to take advantage of the software's nonlinear capabilities. The distinctive elements of mooring system modeling, absent in the conventional Code-Aster workflow, have been incorporated by manually updating the command file with the requisite scripts. The command file adheres to the traditional fundamental stages of numerical simulations, commencing with the assimilation of the mesh, the choice of modeling, and the documentation of moments, materials, and initial and boundary conditions. [45, 47-50]. Initially, the geometrical characteristics of the model were determined with GMSH software, which is a prominent open-source 3D finite element mesh generator. The fundamental aim of this software is to deliver a rapid, agile, and user-friendly meshing tool with the capability of parametric input and flexible visualization. GMSH encompasses four modules, namely geometry, mesh, solver, and post-processing, that form the foundation of its architecture [51].

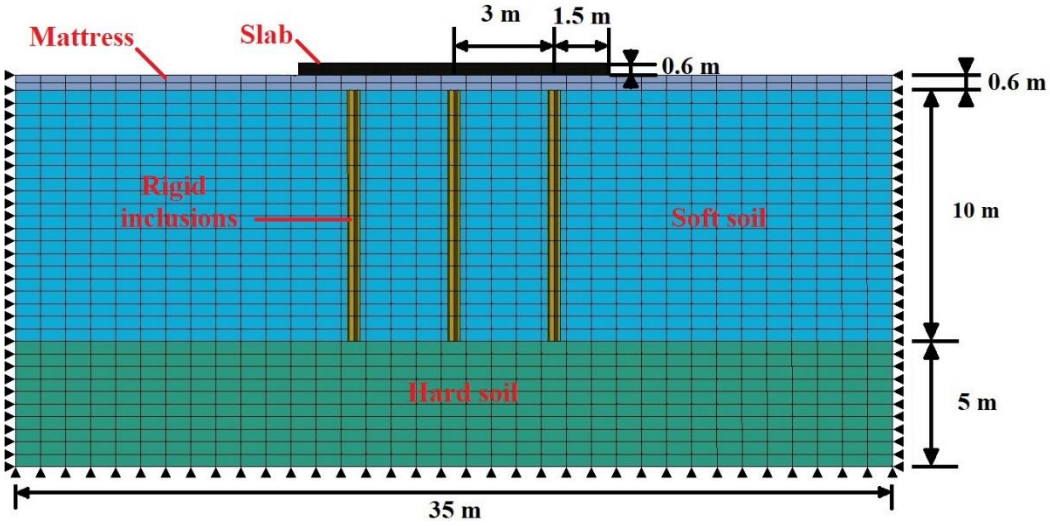


(a)

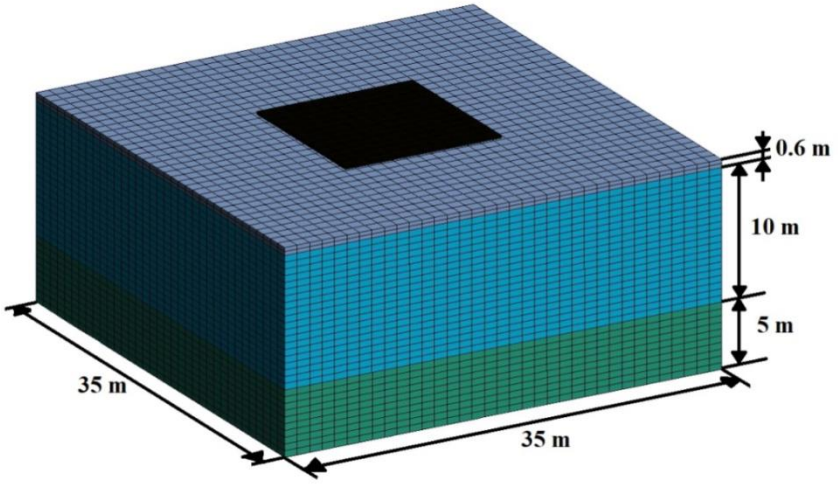


(b)

Fig. 2. Schematic view of the 3D numerical models and mesh distributions: (a) Half model view. (b) 3D view

Figure 2 displays the model implemented in the numerical simulation. The magnitude of the mesh element ought to be minimized such that the mesh may effectively convey waves without any digital distortion. The dimensions of the mesh are contingent on the wave propagation speed and frequencies implicated [40, 44, 52]. Demonstrate that the dimensions of an element must be reduced to a range of one eighth to one tenth of the wavelength λ. As a result, the upper limit of the frequency that can be accurately simulated for a given mesh is established as follows [53]:

$$f = \frac{C_s}{10.\Delta l} \qquad with \qquad f = \frac{\omega}{2\pi} \tag{1}$$

Where, $C_s$: the wave propagation speed, Δl: the dimensions of the mesh component, ω : the excitation frequency.

## 2.4 Physical Models

In this study, six models were questioned while varying the number of inclusions in each model in order to study the impact of the number of inclusions on the overall behavior of the system and on the variation of the stresses taken up by each inclusion. Inclusions are represented in the Code-Aster by linear elements, while the soil and mattress have been represented through volume elements. Meanwhile, shell elements have been used to depict the slab.

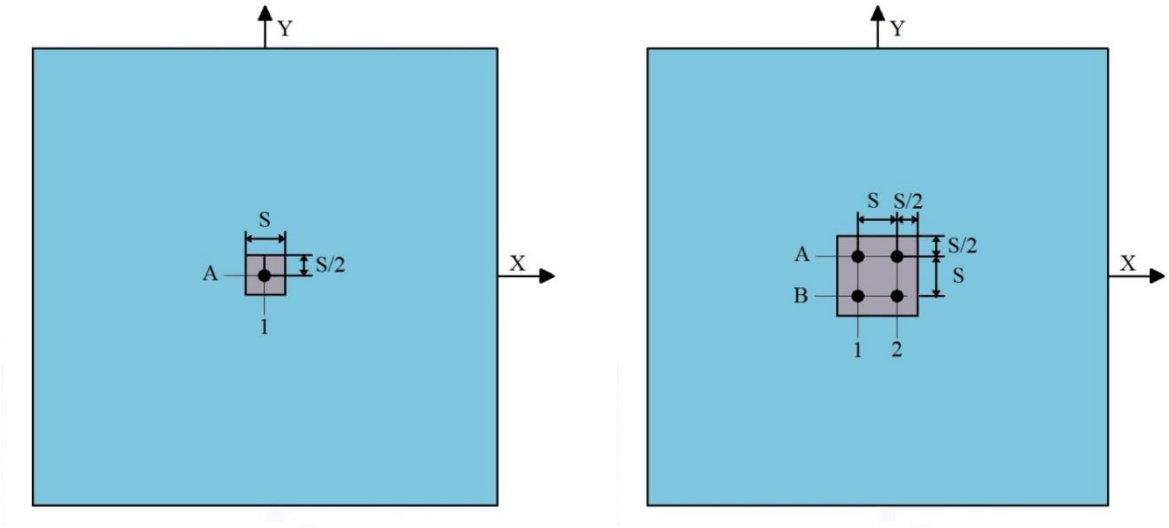


(a) (b)

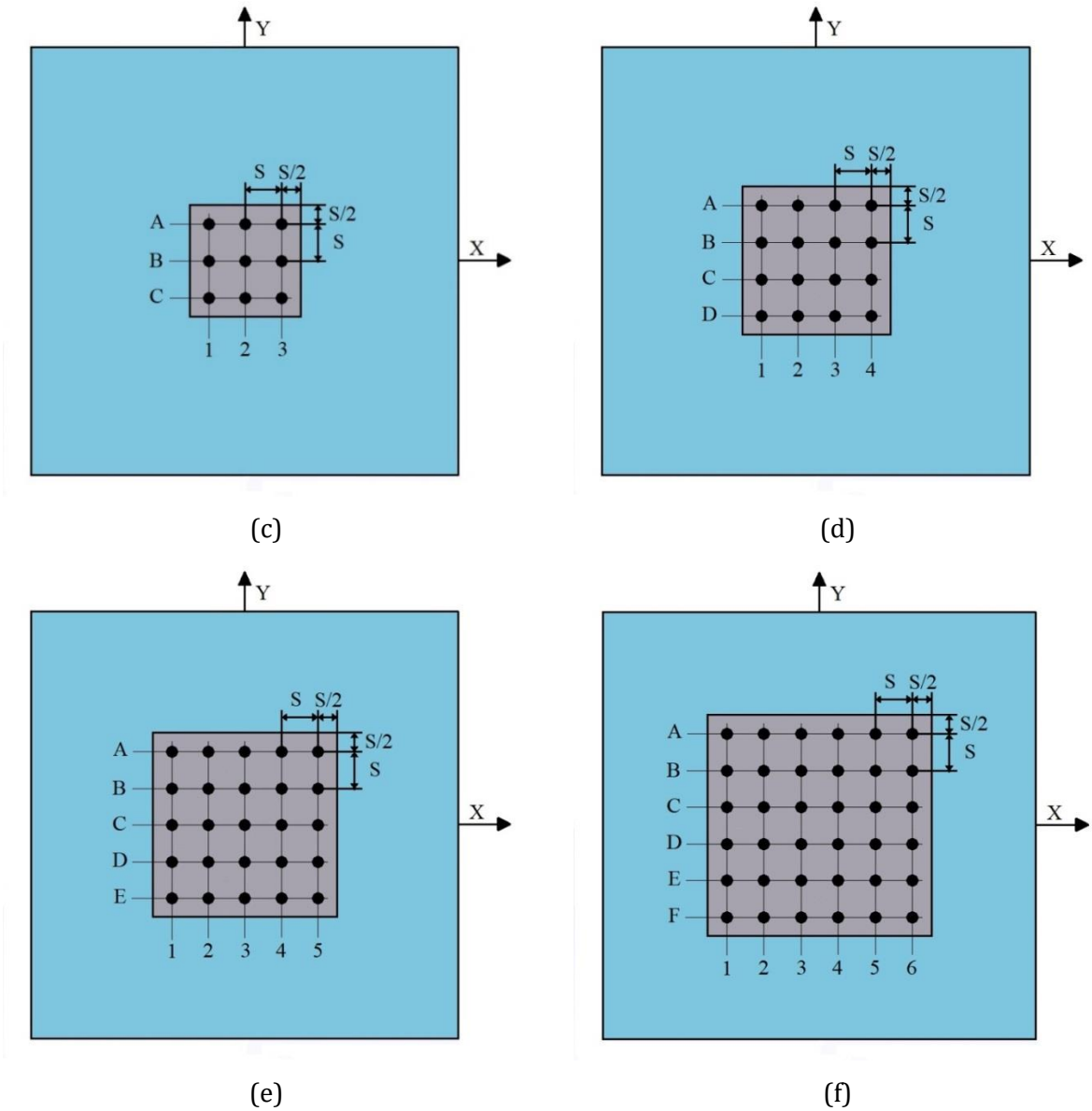


Fig. 3. Plan view of the six numerical models studied: (a) model 1 "one inclusion". (b) model 2 "4 inclusions". (c) model 3 "9 inclusions". (d) model 4 "16 inclusions". (e) model 5 "25 inclusions". (f) model 6 "36 inclusions"

The initial, second, and third models constitute a unified entity, featuring a singular inclusion, a 2x2 matrix of four inclusions, and a 3x3 matrix with a total of nine inclusions, correspondingly. Meanwhile, the fourth, fifth, and sixth models encompass configurations with 16 inclusions arranged in a 4x4 matrix, 25 inclusions forming a 5x5 matrix, and 36 inclusions structured in a 6x6 matrix, respectively. In the context of the first, third, and fifth models, the outcomes are derived from the central inclusion. In contrast, within the second, fourth, and sixth models, the results are determined based on one of the four inclusions situated at the center of the model, owing to their symmetrical arrangement. These models calculate stresses such as shear force and bending moment, as well as displacements, employing the Code-Aster software.

## 2.5 Seismic Loads

The seismic signal utilized in this study corresponds to the seismic activity observed in Nice, France. Its accelerogram aligns with the French design spectrum, as detailed in [54] and It has a maximum acceleration of 0.35g. This accelerogram spans a time history of 21 seconds, and you can find a visual representation of it in Fig. 4.a, Additionally, The Fourier amplitude of the uncorrected Nice record suggests that the maximum frequency fmax is below 5 Hz, as illustrated in Fig. 4.b [55,

56]. To generate comprehensive velocity profiles, our research approach involved amalgamating existing records. Subsequently, all nodes located along the model's lower boundary were subjected to these velocity profiles in the horizontal direction, following the methodology described by [44] We can compute the fundamental frequency of a soil layer using this formula: ω = 4 H/Vs

- H: the soil layer's total depth
- Vs: the shear wave velocity (m/s)

For lower damping values, the resonant frequency is roughly equal to the natural frequency

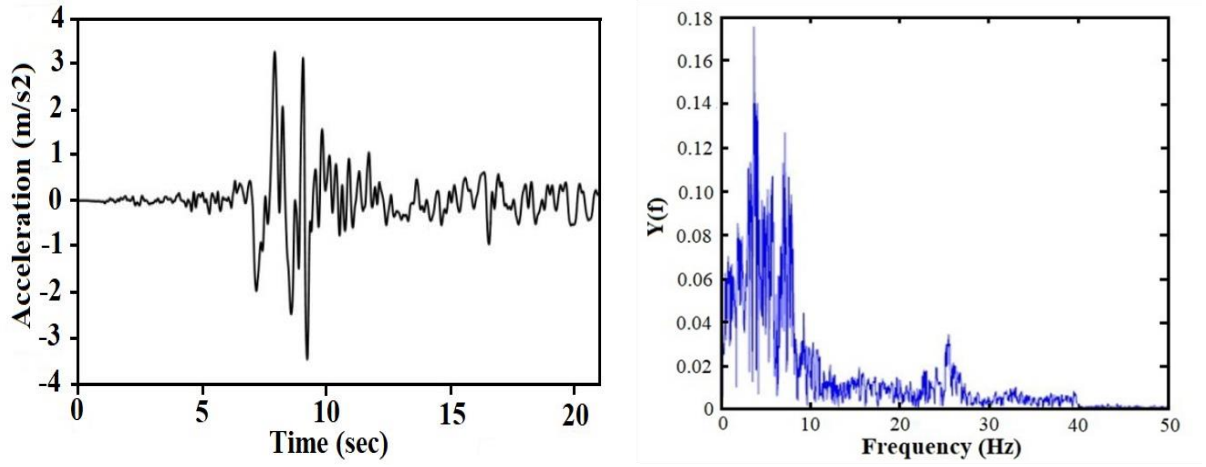


(a) (b)

Fig. 4. Seismic input signals of Nice: (a) Acceleration time history. (b) Fourier amplitude

## 3. Results and Discussion

To justify the proper functioning of the proposed study, the numerical results for the proposed numerical model are compared and validated in the frequency domain with different numerical solutions formulated for pile groups system [44, 57]. The results of the dynamic stiffness matrix $K_{ij}$ of a pile group are in good agreement with the results obtained by [58]. The dynamic impedance of a single pile and a cylinder pile is compared with those obtained by [58-61], respectively.

### 3.1 Non-linear Elastic Domain

In the initial case, the influence of the number of inclusions on stresses such as shear force and bending moment, as well as horizontal displacements in non-linear elastic behavior was examined. The findings for the six models analyzed are presented in Figs. 6 and 7. The curves displayed illustrate the maximum outcomes of the horizontal displacement and stresses (shearing force and bending moment) in the central inclusion for each model based on the depth (i.e., the length of the inclusion).

*3.1.1 The Variation of The Displacement and Internal Forces at The Head of The Central Inclusion as A Function of Time*

Figure 5 illustrates the time-history curve depicting the horizontal displacement and internal forces at the head of the central inclusion in the six models. Within a time, duration of 15 s, with a step of 0.01 s, this figure demonstrates that the evolution of internal forces and displacement aligns with the seismic loading, yielding nearly identical outcomes in all six models. It is worth noting that the initial model featuring a single inclusion exhibits the largest outcomes. As the number of inclusions increases, both the shear forces and bending moments, along with the horizontal displacement, diminish. The maximum results are observed between 7 and 8 seconds according to the time history (Fig. 5).

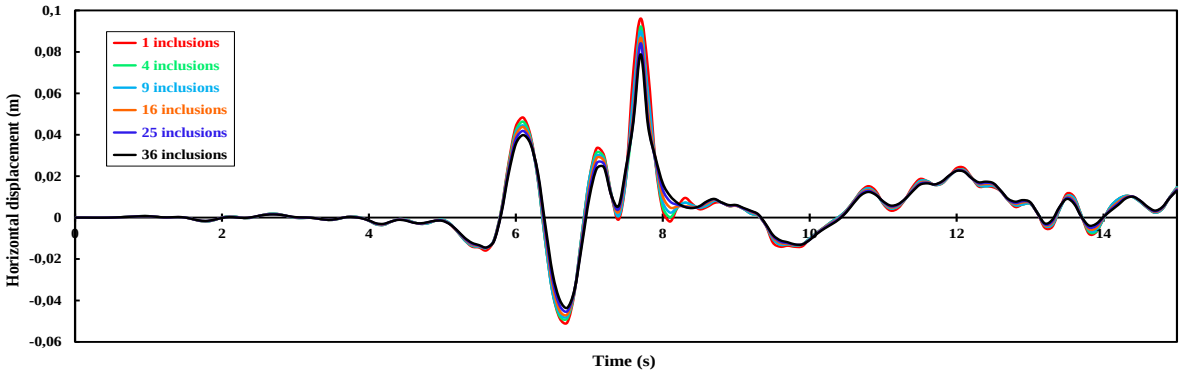


(a)

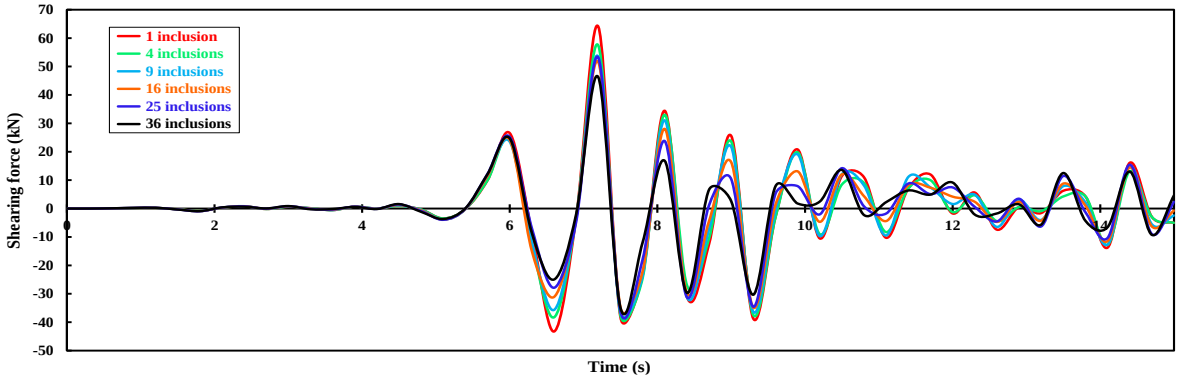


(b)

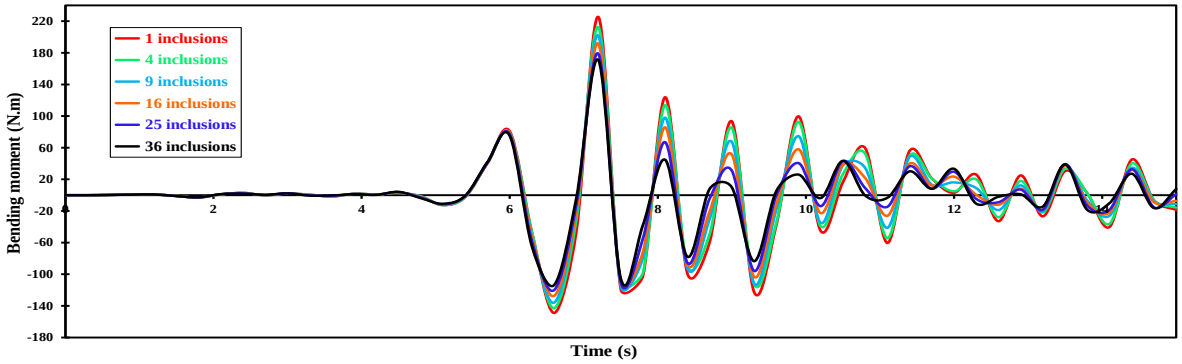


(c)

Fig. 5. The variation of the displacement and internal forces at the head of the central inclusion in the six models as a function of time: (a) Horizontal displacements. (b) Shearing force. (c) Bending moment

### *3.1.2 Horizontal Displacements*

Figure 6 illustrates the displacements within the central inclusions of the six systems as a function of depth. Notably, the displacements within each inclusion exhibit a linear pattern, with the maximum displacement occurring at the head and gradually decreasing towards the minimum value at the tip. To provide specific values, for the "single inclusion" system, the maximum displacement at the inclusion is 0.096 meters at the head and decreases to 0.076 meters at the tip. These results vividly showcase how the number of inclusions within the reinforcing system impacts the variation in displacements. Moreover, it's evident that as the number of inclusions increases, the displacement at the inclusion head consistently decreases. This correlation underscores the influence of the inclusion count on the displacement behavior.

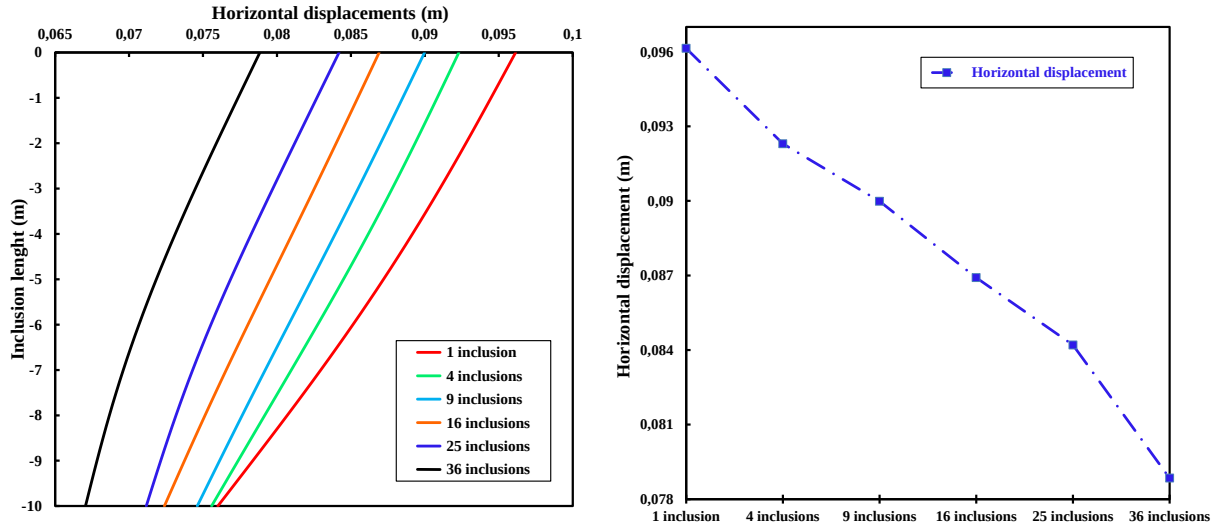


(a) (b)

Fig. 6. Impact of rigid inclusions on reinforcement system behavior: (a) The horizontal displacement of the central rigid inclusions for the 6 models. (b) Variation of the maximum horizontal displacement according to the number of inclusions

### *3.1.3 Bending Moments and Shear Forces*

Figure 7 provides a visual representation of the shear force and bending moment profiles as a function of depth. When examining the central inclusion, which experiences the highest load in each model, a distinctive pattern emerges for the shear force. The shear force displays a linear relationship along the depth, with opposite signs in the upper and lower halves. At the head and foot of the inclusion, the maximum shear force is observed, with the head experiencing a greater force than the foot. This force remains nearly constant for depths shallower than 1 meter and subsequently decreases until it reaches zero at a depth of 4.5 meters, roughly halfway into the inclusion. Beyond this point, the force follows a similar trajectory but with a change in sign until it reaches its maximum value at the foot of the inclusion.

In the first model, specific values recorded for the shear force at different depths include 64 kN at the head, 0 kN at a depth of 5 meters, and -46.9 kN at the tip of the inclusion. These findings provide a comprehensive understanding of how shear forces vary with depth within the central inclusion. The bending moment profile within the inclusion exhibits an almost parabolic relationship, characterized by values of zero at both the top and bottom, with the peak typically occurring at the midpoint of the inclusion. A noteworthy example is observed in the "inclusion B2" within the third model, where the maximum bending moment reaches 160 kN at a depth of 5 meters. This phenomenon can be attributed to the absence of recesses or supports at the ends of the inclusion, causing it to behave akin to a simply supported beam. As a result, the bending moment distribution follows a classic parabolic pattern, with the highest moment occurring at the midpoint, a hallmark of such structural configurations.

Figures 7.c and 6.d provide a comprehensive view of the maximum variation in shear force and bending moment for each model, respectively. The values are determined from the head for shear force and at a depth of 5 meters for bending moment.

A consistent trend emerges from these figures, revealing that as the number of inclusions increases, the internal stresses decrease. This observation holds true for each individual computation, as depicted in the presented figures. Both the magnitudes of stresses and horizontal displacements show a diminishing trend with the progressive increase in the number of inclusions. This reduction in stress and displacement can be attributed to the fact that the total stress is distributed among all the inclusions within the system. Consequently, when the number of inclusions is augmented, the resultant stresses undergo a decrease, leading to a more evenly distributed load across the system.

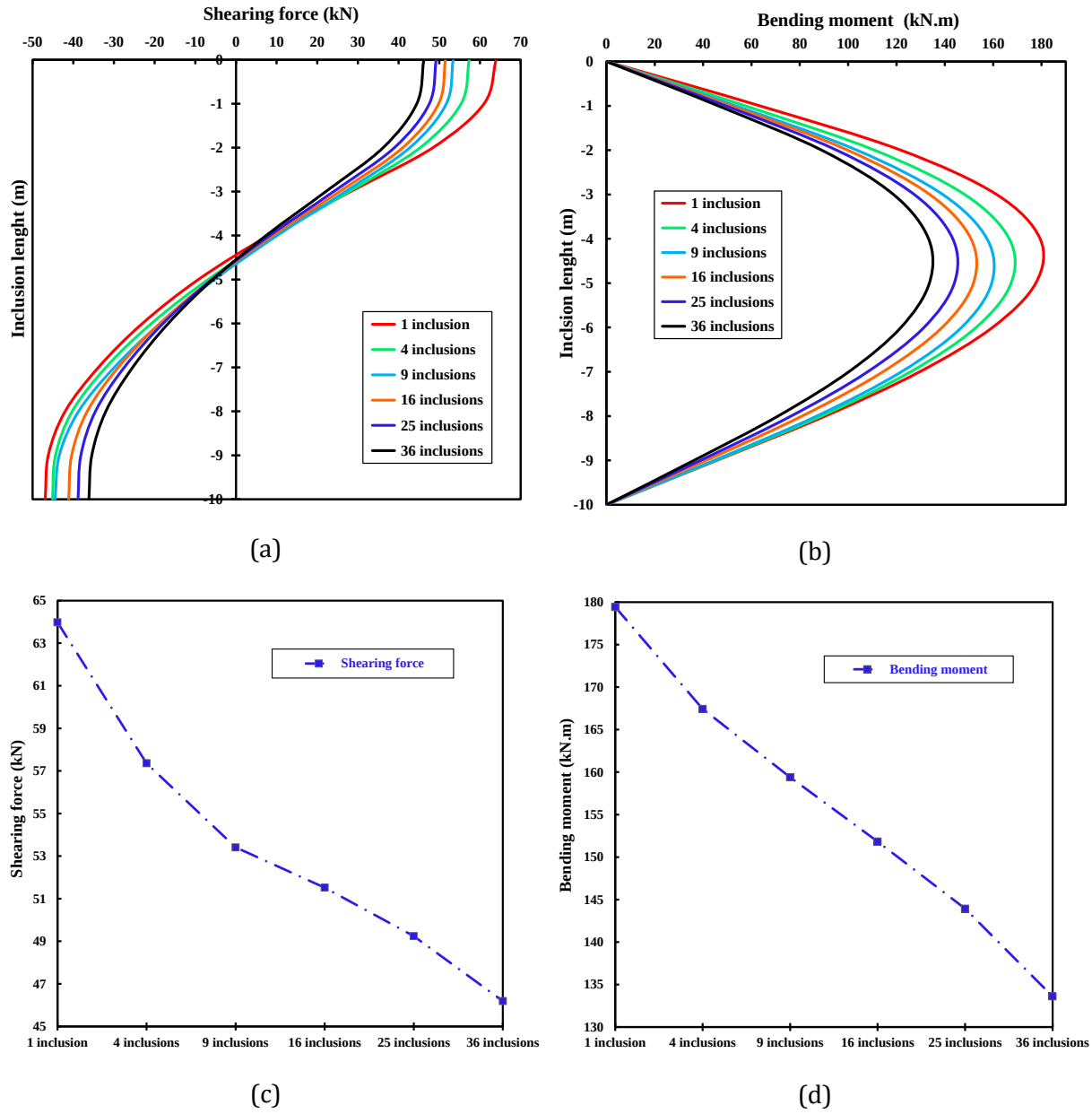


Fig. 7. Shearing force and bending moment: (a) Shearing force in the most solicited inclusion for the 6 models. (b) Bending moment in the most stressed inclusion for the 6 model. (c) Maximum shearing force for each inclusion, (at the head). (d) Maximum bending moment for each inclusion, (at 5 m)

### *3.1.4 The Effect of Inclusion Depth on The Variation of Displacements and Stresses*

Figure 8 provides a comprehensive overview of horizontal displacement and stresses recorded at depths of 0 meters (the head of the inclusion), 2 meters, 5 meters, and 8 meters, focusing on the most stressed inclusion in each model. Several noteworthy trends can be observed: Decrease with Increased Inclusions: Across all depths, there is a consistent decrease in both displacements and stresses as the number of inclusions increases. This suggests that the addition of more inclusions in the system leads to a reduction in the observed displacements and stresses.

Horizontal displacement shows a diminishing trend as depth increases. For instance, in "model 3," the horizontal displacement of inclusion B2 measures 0.090 m at 0 meters, 0.087 m at 2 meters, 0.082 m at 5 meters, and 0.078 m at 8 meters. This indicates a decrease in horizontal displacement with greater depth. The bending moments exhibit a characteristic progression, starting from zero, reaching a maximum at the midpoint (5 meters), and then gradually decreasing. For example, in

the second model, the recorded bending moments at depths of 2 meters, 5 meters, and 8 meters are 111 kN.m, 167 kN.m, and 88.9 kN.m, respectively.

The shearing force profile differs from the bending moment. Initially, it decreases from the apex of the inclusion towards the center, nearly reaching zero. As an example, in the fifth model, inclusion C3 exhibits a force of 49.2 kN at the head of the inclusion and 39 kN at a depth of 2 meters, -5.95 kN at 5 meters, and subsequently increases while traversing almost identical values as observed in the upper region. At a depth of 8 meters, the shearing force equals -34.56 kN. These observations collectively highlight the influence of inclusion count and depth on displacement, bending moment, and shearing force patterns within the studied models.

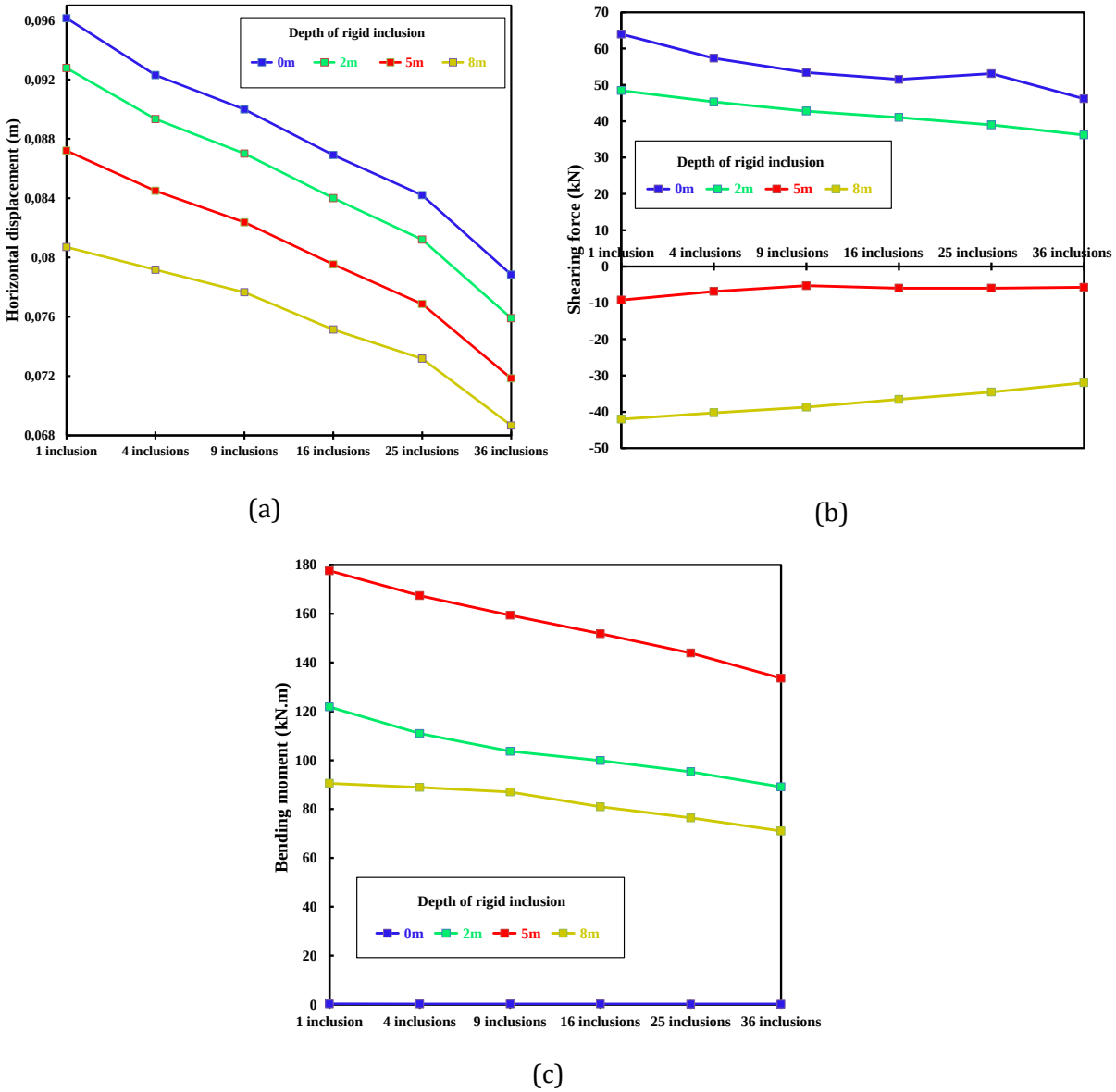


Fig. 8. The effect of inclusion depth on variation in displacements and stresses: (a) Horizontal displacement. (b) Shearing force. (c) Bending moment

### *3.1.5 The Effect of The Inclusion Network's Position on The Horizontal Displacements and Solicitations*

In order to assess the significance of inclusion placement on the variability of displacement and forces, we conducted an analysis by comparing the results obtained for the central-line inclusions of models 5 and 6:

- Model 5 (inclusions: C1, C2, and C3).

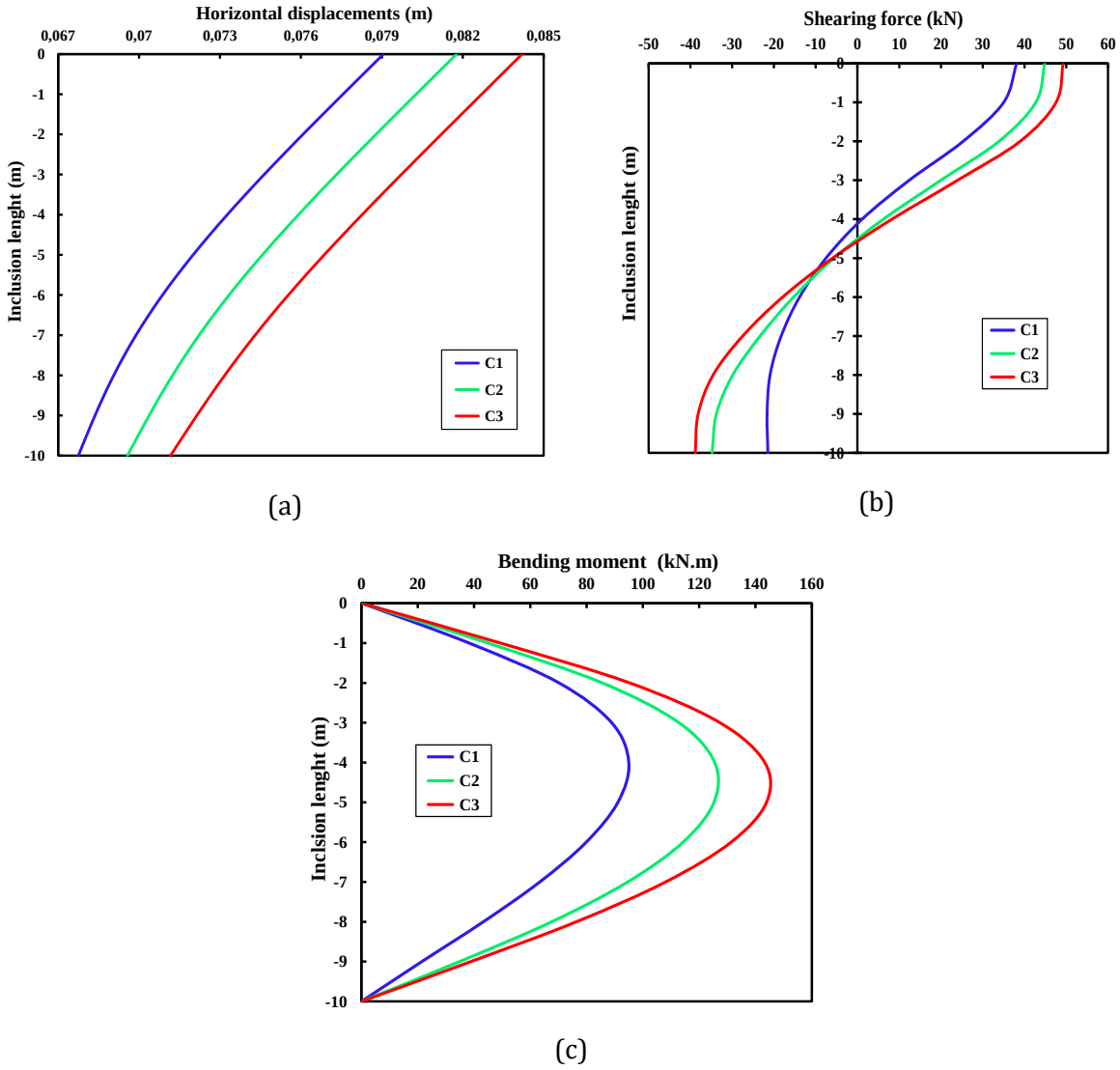


Fig. 9. The results of the central line inclusions according to the depth: (a) Horizontal displacement. (b) Shearing force. (c) Bending moment

- Model 6 (inclusions: D1, D2, and D3)

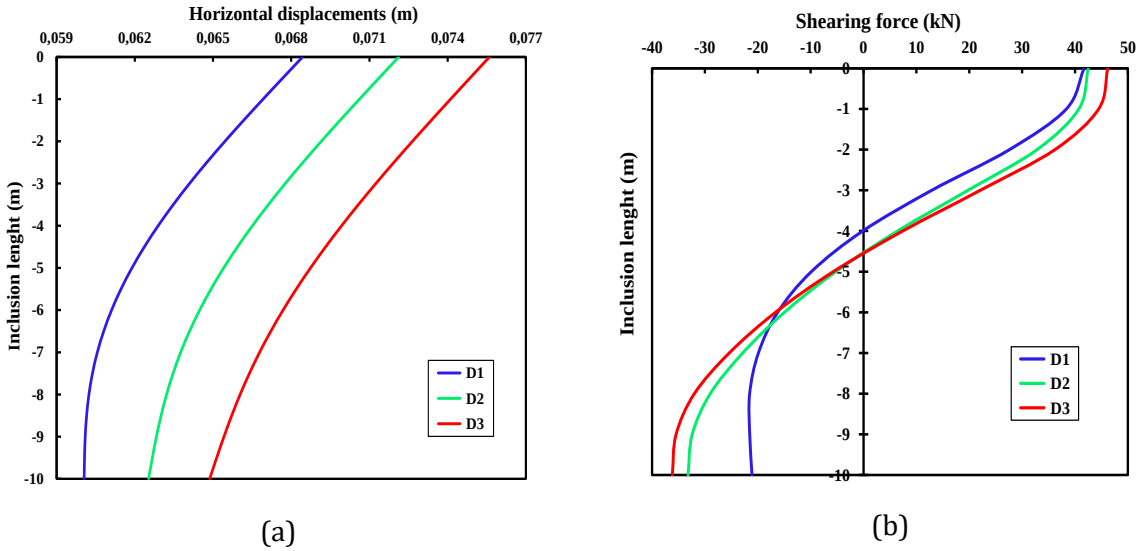

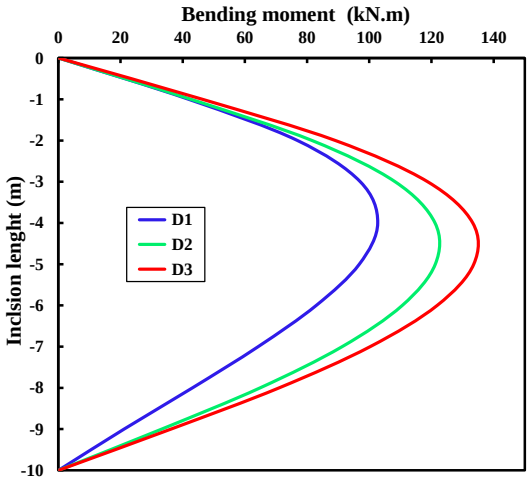


(c)

Fig. 10. The results of the central line inclusions according to the depth: (a) Horizontal displacement. (b) Shearing force. (c) Bending moment

Figures 9 and 10 present a detailed overview of the horizontal displacements and stresses (shear forces and bending moments) along the central line of each model. Several key observations can be made from this analysis: It's important to note that all inclusions along the central line maintain a consistent spacing. A consistent trend is evident where horizontal displacements and stresses decrease as the inclusions approach the edge of the model. This phenomenon can be attributed to the application of earthquake forces to the middle of the substrate base, which is in contact with the soft soil. For instance, in model 5, at the head of the central line, inclusion C3 (located at the center of the model) records a horizontal displacement of 0.084 m. In comparison, inclusion C2 exhibits a displacement of 0.082 m, and inclusion C1 registers a lower value of 0.079 m. This trend highlights that the central inclusion experiences higher displacement compared to those further from the center. In model 6, at a depth of 8 meters, inclusion D3 shows a shearing force of -32 kN, inclusion D2 experiences -29 kN, while inclusion D1 has -21.5 kN. Regarding the bending moment at a depth of 2 meters in the same model, inclusion D3 records the highest value of 89.11 kN.m, followed by inclusion D2 at 81.61 kN.m, and inclusion C1 at 76.92 kN.m.

Central Inclusion Vulnerability: These results collectively indicate that the central inclusion is more susceptible to displacement and stress concentrations when compared to the other inclusions. The internal stresses decrease, and horizontal displacement reduces as one moves away from the center of the model, underscoring the importance of inclusion placement in assessing structural vulnerability. These findings contribute to a better understanding of how inclusion positioning impacts the behavior of the model under seismic loading, shedding light on the distribution of forces and displacements along the central line.

### 3.2 Elasto-Plastic Behavior

The investigation in question delves into the influence of different inclusion quantities on horizontal displacements and stresses, encompassing shear forces and bending moments. This analysis considers the elasto-plastic behavior of the soil. The curves presented in the following figures showcase the maximum results, which correspond to inclusions positioned in the middle, for each of the six models being studied. These curves are plotted with respect to depth, specifically the length of the inclusion. Subsequently, the maximum values are compared across each case to assess the impact of varying inclusion quantities on the observed outcomes.

Figures 11.a, 12.a, and 11.b provide a detailed illustration of the variations in displacement and stress (including bending moments and shear forces) concerning the depth of the most stressed inclusion for each corresponding model. Here are some key observations:

The displacement curve does not follow a linear pattern, unlike the initial behavior of the soil. Instead, it exhibits higher displacement values. This suggests that the soil behaves differently with

increased displacement values. The shear force curve showcases a distinctive pattern. Initially, it is relatively low at the inclusion head, followed by an increase to a peak value at a depth of 5 meters. Subsequently, it decreases to zero at 7 meters before rising again, with a different signal pattern towards the inclusion bottom. This complex behavior suggests changing forces within the soil layers. The bending moment follows an almost parabolic relationship, with the maximum value occurring at 7 meters and values of zero at both the top and bottom. For instance, in the case of "inclusion B2" within the third model, the maximum bending moment reached 129.4 kN.m at a depth of 7 meters.

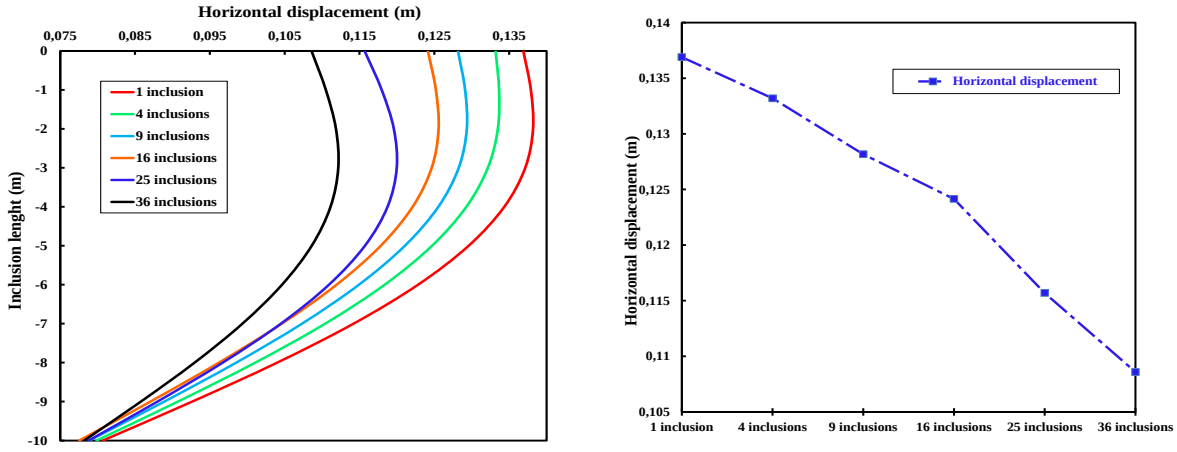


(a) (b)

Fig. 11. Impact of rigid inclusions on reinforcement system behavior: (a) The horizontal displacement of the central rigid inclusions for the 6 models. (b) Variation of the maximum horizontal displacement according to the number of inclusions

Now, turning to Figures 11.b, 12.c, and 12.d, these graphs display the maximum values of displacements and stresses for each model. The following observations can be made: It's evident that horizontal displacement, shear force, and bending moment exhibit an inverse proportionality concerning the increase in the number of inclusions. As the number of inclusions increases, the maximum values of these parameters decrease. This suggests that adding more inclusions leads to a reduction in displacement and stress levels, highlighting the effectiveness of inclusion strategies in mitigating structural loads and deformations. These findings contribute to a deeper understanding of the complex behaviors of soil, shear forces, and bending moments, and how they are influenced by the number of inclusions in the system.

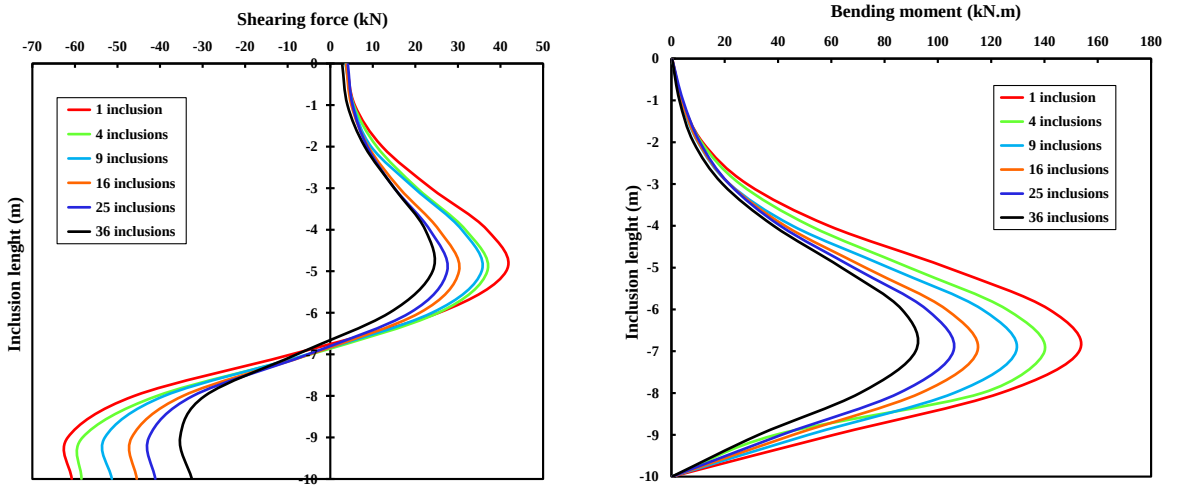


(a) (b)

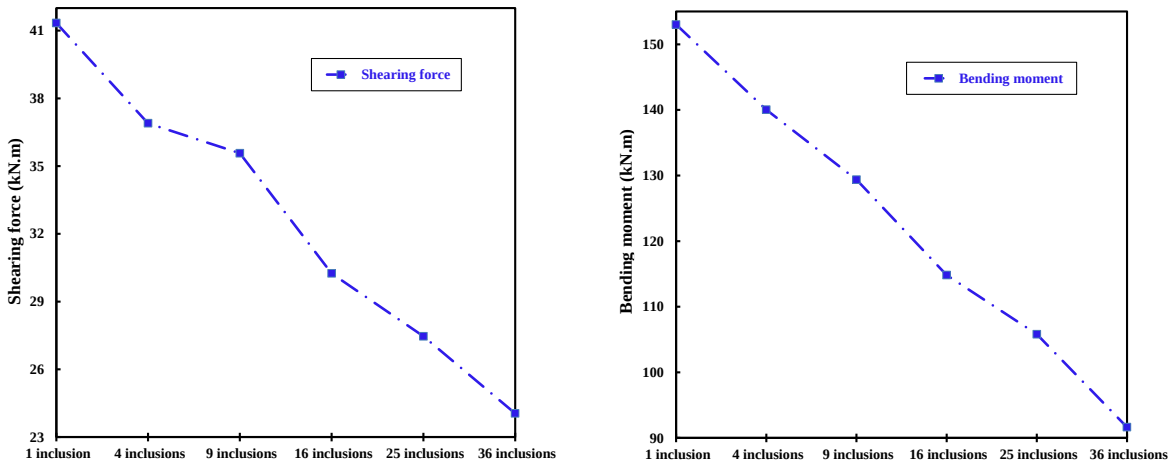


(c) (d)

Fig. 12. Bending moment and shearing force results in elasto-plastic behavior: (a) Variation of the shearing force according to the depth in the central inclusion for each model. (b) Variation of the bending moment as a function of the depth in the central inclusion for each mod. (c) Maximum shearing force (at the head of the central inclusion), for each model. (d) Maximum bending moment (at 5 M), for each model

## 3.3 Comparison Between Non-Linear Elastic and Elasto-Plastic Behavior

### *3.3.1 Comparison of The Maximum Results in Each Model*

We examined the greatest outcomes in each model for displacement and internal forces in Fig.13 and Table 2 after computing each behavior separately. Figure 13.a indicates that the maximum values of the horizontal displacement in elasto-plastic behavior are larger than those of elastic behavior. Conversely, when we compared the results of bending moments and shear forces, we found that the elastic behavior had the largest values, as shown in Figure 13.b.

Table 2. The maximum results of each model in the two behaviors

| | Horizontal displacement $\times 10^{-2}$ (m) | | Shearing force $\times 10^{3}$ (N) | | Bending moment $\times 10^{3}$ (N·m) | |
|---|---|---|---|---|---|---|
| | Elastic | Elasto-plastic | Elastic | Elasto-plastic | Elastic | Elasto-plastic |
| 1 inclusion | 9,61 | 13,69 | 63,98 | 41,34 | 179,43 | 153,02 |
| 4 inclusions | 9,23 | 13,32 | 57,36 | 36,90 | 167,44 | 140,03 |
| 9 inclusions | 8,99 | 12,82 | 53,41 | 35,58 | 159,40 | 129,37 |
| 16 inclusions | 8,69 | 12,41 | 51,52 | 30,25 | 151,83 | 114,82 |
| 25 inclusions | 8,42 | 11,57 | 49,24 | 27,46 | 143,93 | 105,81 |
| 36 inclusions | 7,88 | 10,86 | 46,19 | 24,05 | 133,60 | 91,63 |

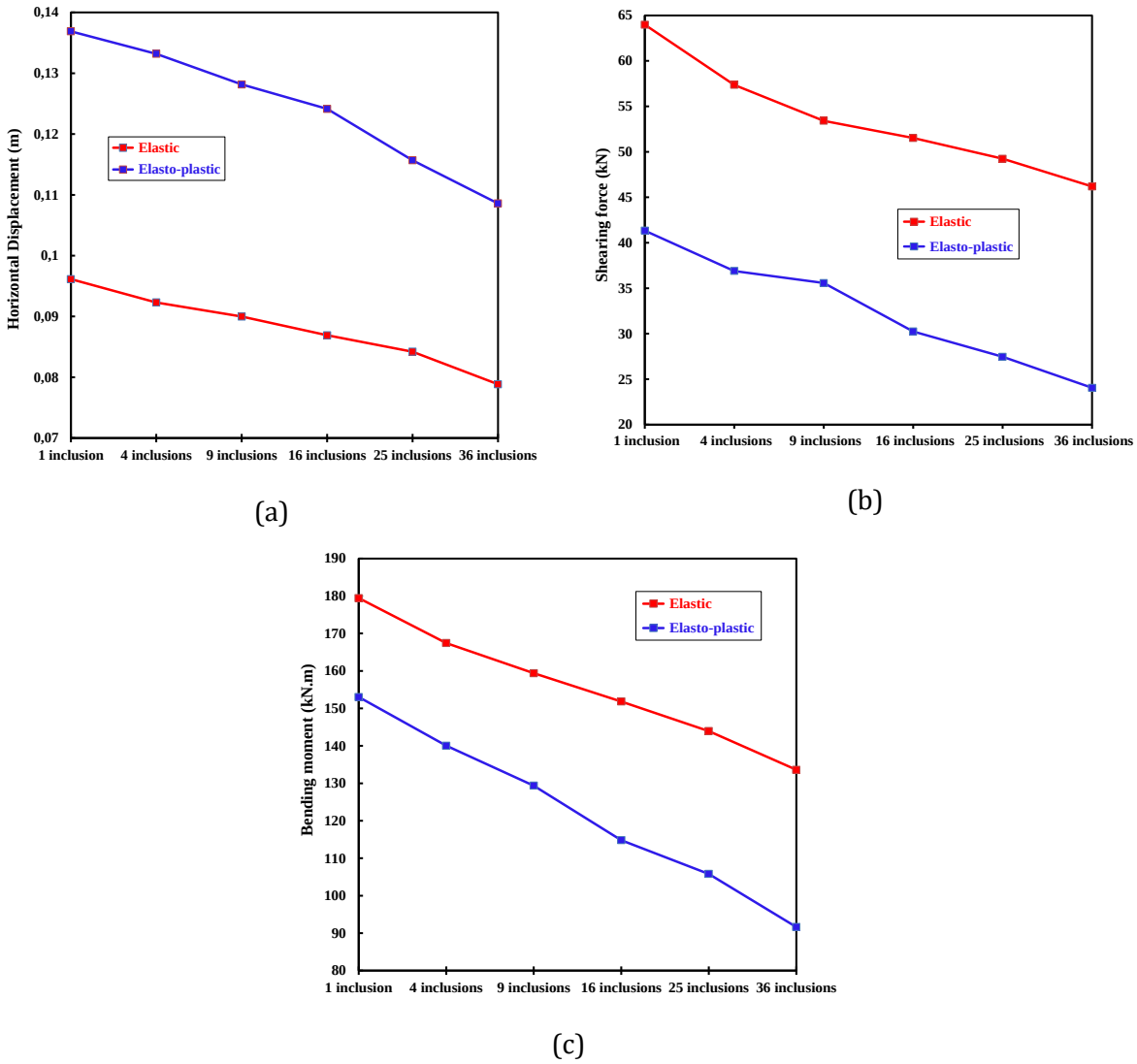


Fig. 13. Comparison between the maximum results of each model in non-linear elastic and elasto-plastic behavior: (a) Horizontal displacement. (b) Shearing force. (c) Bending moment

### *3.3.2 Comparison Between the Results of Model 4 In the Two Behaviors*

In this section, we compare the results between the non-linear elastic and elasto-plastic behaviors of the soil using Model 4, which contains 16 inclusions. Figure 14 and Table 3 depicts the variations in displacement and internal stresses (including bending moments and shear forces) for both cases (non-linear elastic and elasto-plastic) with respect to the length of the inclusion. This comparison allows us to assess how the two different soil behaviors impact the structural response. Please refer to Figure 14 and Table 3 to analyze and interpret the specific findings and differences between the non-linear elastic and elasto-plastic simulations for Model 4.

The comparison between the results obtained for the non-linear elastic and elasto-plastic behaviors reveals notable differences. Here are the key findings from this comparison; horizontal Displacement (Fig. 14.a). In the elasto-plastic behavior case, horizontal displacement values are significantly higher than those observed in the non-linear elastic behavior. Furthermore, the displacement curves are not linear in the elasto-plastic case, indicating more pronounced deformation and structural response under elasto-plastic soil behavior.

Table 3. The results of the non-linear elastic and elasto-plastic behavior as a function of the depth in inclusion C2 of the 4th model.

| Behavior | Depth (m) | Horizontal displacements × $10^{-2}$ (m) | Shearing force × $10^{3}$ (N) | Bending moment × $10^{3}$ (N·m) |
|---|---|---|---|---|
| Elastic | 0 m | 8,69 | 51,52 | 0,146 |
| | 3 m | 8,25 | 25,46 | 133,78 |
| | 5 m | 7,95 | -59,57 | 151,83 |
| | 7 m | 7,66 | -28,95 | 114,43 |
| | 10 m | 7,24 | -41,13 | 0,071 |
| Elasto-plastic | 0 m | 12,41 | 36,91 | 0,19 |
| | 3 m | 12,47 | 16,25 | 21,79 |
| | 5 m | 11,79 | 30,25 | 72,80 |
| | 7 m | 10,46 | -48,12 | 114,82 |
| | 10 m | 7,75 | -45,47 | 0,18 |

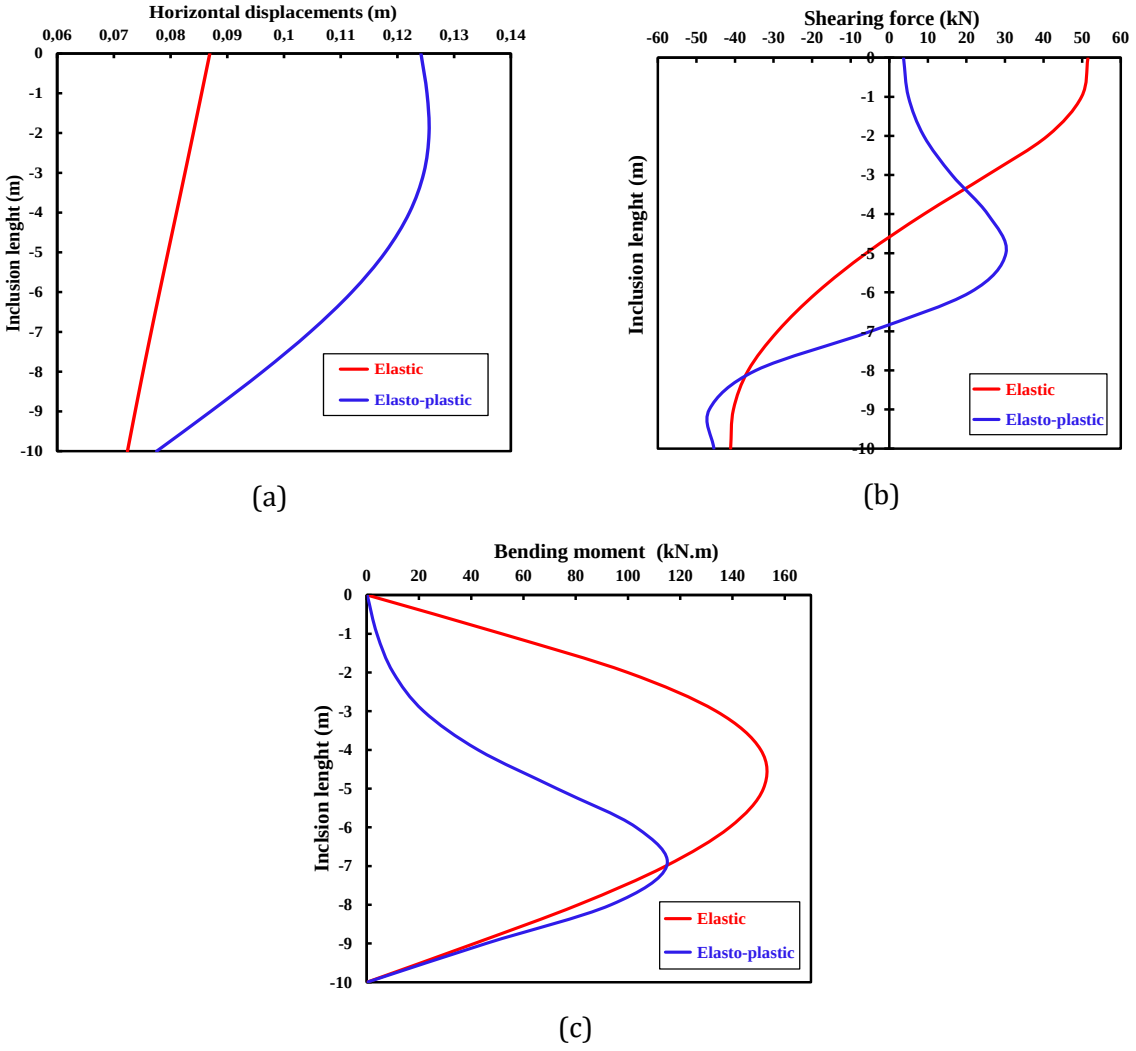


Fig. 14. The results of the comparison between non-linear elastic and elasto-plastic behavior as a function of the depth in inclusion C2 of the 4th model: (a) Horizontal displacements. (b) Shearing force. (c) Bending moment

In the non-linear elastic behavior, shear forces exhibit a peak value at the head of the inclusion, decrease towards zero at the middle, and then increase with negative values towards the bottom, though still lower than the top of the inclusion. In the elasto-plastic behavior, shear forces show weaker values at the inclusion head, followed by a gradual escalation towards the highest value at the midpoint. The shear forces then reach zero at a depth of 7 meters. This behavior suggests that under elasto-plastic conditions, there is a redistribution of forces with depth.

In the non-linear elastic behavior, the bending moment attains its maximum value at approximately the middle of the inclusion, reaching 152 kN.m. In the elasto-plastic behavior, the bending moment reaches its peak at a depth of 7 meters, corresponding to a value of 115 kN.m. Additionally, at the top and bottom of the inclusion, the values are nearly zero. This indicates that the elasto-plastic behavior leads to a different distribution of bending moments compared to non-linear elastic behavior.

Overall, the comparison underscores significant differences in the structural response between the non-linear elastic and elasto-plastic soil behaviors. The elasto-plastic behavior results in higher horizontal displacements, while the non-linear elastic behavior leads to higher shearing forces and bending moments. These findings emphasize the importance of considering soil behavior when assessing the response of structures subjected to seismic forces.

## 4. Conclusions

This article focuses on analyzing the behavior of reinforced soil with rigid inclusions under seismic stress conditions. The study particularly examines the influence of these inclusions on the reinforcement system, employing three-dimensional finite element numerical models with absorbing boundaries based on the direct method. The numerical models simulate various quantities of rigid inclusions, and horizontal displacements, as well as internal stresses, are computed using the Code-Aster software. The analysis takes into account two different types of soil behavior: non-linear elastic and elasto-plastic. Six different models are studied in this research, each varying in the number of inclusions.

The findings from this investigation can be summarized as follows:

- 1. Inclusion Quantity Effect: Increasing the number of inclusions within the system results in a reduction of stresses and horizontal displacements within these inclusions. This suggests that a higher number of inclusions contribute to a more effective reinforcement of the soil system under seismic forces.
- 2. Influence of Inclusion Position: Inclusions situated closer to the shore of the inclusion network, away from the point of applied load, experience lower stresses and horizontal displacements compared to those positioned at the center of the network. This highlights the significance of inclusion placement in the reinforcement system's response.
- 3. Comparison of Soil Behaviors: The study considers two soil behaviors, non-linear elastic and elasto-plastic. It is observed that in elasto-plastic soil behavior, the soil is more deformable, and its resistance is smaller than in the non-linear behavior.
- 4. Bending moments reach their maximum values at different depths in the two cases, with non-linear elastic behavior peaking at 5 meters and elasto-plastic behavior at 7 meters, albeit at a lower value.
- 5. The curve of shear force also exhibits distinct patterns in the two cases, with non-linear elastic soil showing a peak at the head of the inclusion and decreasing to zero at 5 meters, while elasto-plastic soil reaches zero at 7 meters.
- 6. Horizontal displacements differ in magnitude and curve shape between the two soil behaviors, with non-linear elastic soil following a linear curve and elasto-plastic soil exhibiting a non-linear trajectory.
- 7. In summary, this research provides valuable insights into the behavior of reinforced soil under seismic loading conditions, with a focus on the influence of rigid inclusions and the effects of different soil behaviors. The findings emphasize the importance of inclusion count, placement, and soil behavior in determining the structural response of such systems.

## Acknowledgement

This work was supported and funded by the Directorate General for Scientific Research and Technological Development (DGRSDT, Algeria) and the Civil and Environmental Engineering Laboratory (LGCE) at the University of Jijel. These supports made this study and further research possible.

## References

[1] Jenck O, Dias D, Kastner R. Two-dimensional physical and numerical modeling of a pile-supported earth platform over soft soil. J Geotech Geoenviron Eng. 2007 Mar;133(3):295-305. https://doi.org/10.1061/(ASCE)1090-0241(2007)133:3(295)

[2] Jenck O, Dias D, Kastner R. Three-dimensional numerical modeling of a piled embankment. Int J Geomech. 2009 May;9(3):102-12. https://doi.org/10.1061/(ASCE)1532-3641(2009)9:3(102)

[3] Briançon L, Dias D, Simon C. Monitoring and numerical investigation of a rigid inclusions-reinforced industrial building. Can Geotech J. 2015 Oct;52(10):1592-604. https://doi.org/10.1139/cgj-2014-0262

[4] Zhang J, An L, Li C, Dias D, Jenck O. Artificial neural network response assessment of a single footing on soft soil reinforced by rigid inclusions. Eng Struct. 2023 Apr;281:115753. https://doi.org/10.1016/j.engstruct.2023.115753

[5] Jenck O, Dias D. Modélisations physiques et numériques d'un matelas granulaire érigé sur sol compressible renforcé par inclusions rigides. Rev Fr Geotech. 2009;(126-127):77-91. https://doi.org/10.1051/geotech/2009126077

[6] Mánica Malcom MÁ, Ovando-Shelley E, Botero Jaramillo E. Numerical study of the seismic behavior of rigid inclusions in soft Mexico City clay. J Earthquake Eng. 2016 Apr;20(3):447-75. https://doi.org/10.1080/13632469.2015.1085462

[7] Nunez MA, Briançon L, Dias D. Analyses of a pile-supported embankment over soft clay: Full-scale experiment, analytical and numerical approaches. Eng Geol. 2013 Feb;153:53-67. https://doi.org/10.1016/j.enggeo.2012.11.006

[8] López Jiménez GA, Dias D, Jenck O. Effect of the soil-pile-structure interaction in seismic analysis: case of liquefiable soils. Acta Geotech. 2019 Oct;14(5):1509-25. https://doi.org/10.1007/s11440-018-0746-2

[9] Brûlé S, Plomteux C. Fondations sur sol amélioré dans la masse et renforcé par inclusions souples. In: Procédés d'amélioration et de renforcement de sols sous actions sismiques, GUIDE AFPS/CFMS, Journée du nombre. France; 2012.

[10] Briançon L, Simon B, Thorel L. Le projet ASIRI+ : Amélioration et Renforcement des Sols par Inclusions RIgides. In: Journées Nationales de Géotechnique et de Géologie de l'Ingénieur - Lyon 2020; Lyon, France. 2020.

[11] Messioud S, Neghmouche Y. 3D numerical modeling of soft soil improved by rigid inclusions supported an embankment. Eng Technol J. 2022 May;40(5):636-48. https://doi.org/10.30684/etj.2021.132023.1083

[12] Zhang J, Dias D, Jenck O. 3D numerical modeling of a rigid inclusion reinforced railway embankment under cyclic loading. Transp Geotech. 2023 Jul;41:101003. https://doi.org/10.1016/j.trgeo.2023.101003

[13] Briançon L, Simon B. Performance of pile-supported embankment over soft soil: Full-scale experiment. J Geotech Geoenviron Eng. 2012 Apr;138(4):551-61. https://doi.org/10.1061/(ASCE)GT.1943-5606.0000561

[14] Jenck O. Modélisation physique et numérique du renforcement des sols compressibles par inclusions rigides verticales. In: XXIIIiemes Rencontres Universitaires de Génie Civil 2005 - PRIX JEUNES CHERCHEURS. France; 2005.

[15] Davidovici V, Lambert S. Fondations et procédés d'amélioration du sol: Guide d'application de l'Eurocode 8 (parasismique) (French Edition). Paris: Eyrolles; 2013.

[16] Zhang J, Jenck O, Dias D. 3D numerical analysis of a single footing on soft soil reinforced by rigid inclusions. Int J Geomech. 2022 Aug;22(8):04022113. https://doi.org/10.1061/(ASCE)GM.1943-5622.0002412

[17] Mourya VK, Pandey G, Patel D, Kumar R. Approaches considering non-linearity in soilfoundation-interaction: A State-of-the-Art Review. Res. Eng. Struct. Mater., 2023; 9(3): 989- 1013. http://dx.doi.org/10.17515/resm2023.646me0117

[18] Blasone V, Huseynli S, De Luca F, Karamitros D, De Risi R, Spacone E. Incorporating soil-structure interaction into simplified numerical models for fragility analysis of RC structures. Earthq Eng Struct Dyn. 2025 Feb;54(2):393-412. https://doi.org/10.1002/eqe.4259

[19] Vaziri SJ, Vahdani R, Souri O. Seismic evaluation of BRBF steel structures with L-shaped irregular plan considering soil-structure interaction. Bull Earthquake Eng. 2024;22(10):5347-77. https://doi.org/10.1007/s10518-024-01963-4

[20] Hokmabadi AS, Fatahi B, Samali B. Physical modeling of seismic soil-pile-structure interaction for buildings on soft soils. Int J Geomech. 2015 Apr;15(2):04014046. https://doi.org/10.1061/(ASCE)GM.1943-5622.0000396
[21] Bakhshpoori T, Nezhad ARN. Effects of near-field earthquakes, connection types, and SSI on seismic performance of SMRF. Structures. 2024 Mar;61:105987. https://doi.org/10.1016/j.istruc.2024.105987
[22] Dhadse GD, Ramtekkar G, Bhatt G. Influence due to interface in finite element modeling of soil-structure interaction system: a study considering modified interface element. Res Eng Struct Mater. 2021. https://doi.org/10.1007/s11831-020-09505-2
[23] McKay K. Three applications of the reciprocal theorem in soil-structure interaction [dissertation]. Los Angeles (CA): University of Southern California; 2009.
[24] Messioud S, Sbartai B, Dias D. Effect of seismic oblique waves on dynamic response of an embedded foundation. ISET J Earthquake Technol. 2012 Mar-Jun;49(1-2):37-52. Paper No. 520.
[25] Jarrahi H, Asadi A, Khatibinia M, Etedali S, Paknehad S. Soil-structure interaction effects on the seismic performance of steel moment-resisting frames equipped with optimal rotational friction dampers. Structures. 2022 Sep;43:449-64. https://doi.org/10.1016/j.istruc.2022.05.118
[26] Messioud S. Étude de l'interaction sol-fondation 3D sous sollicitations sismiques [dissertation]. Skikda (Algeria): Université 20 Août 1955-Skikda; 2014.
[27] Van Nguyen Q, Fatahi B, Hokmabadi AS. Influence of size and load-bearing mechanism of piles on seismic performance of buildings considering soil-pile-structure interaction. Int J Geomech. 2017 Jul;17(7):04017007. https://doi.org/10.1061/(ASCE)GM.1943-5622.0000869
[28] Cheshmehkaboodi N, Guizani L, Ghlamallah N. Soil-structure interaction effects on seismic responses of a conventional and isolated bridge subjected to moderate near-fault and far-field records. CivilEng. 2023 Jun;4(3):702-25. https://doi.org/10.3390/civileng4030040
[29] Romanel C, Kundu T. A hybrid modelling of soil-structure interaction problems for deeply embedded structures in a multilayered medium. Earthq Eng Struct Dyn. 1993 Jul;22(7):557-71. https://doi.org/10.1002/eqe.4290220702
[30] Spyrakos CC, Xu C. Dynamic analysis of flexible massive strip-foundations embedded in layered soils by hybrid BEM-FEM. Comput Struct. 2004 Nov;82(29-30):2541-50. https://doi.org/10.1016/j.compstruc.2004.05.002
[31] Tyapin A. Soil-structure interaction. In: Sezen H, editor. Earthquake Engineering. Rijeka (Croatia): InTech; 2012. https://doi.org/10.5772/48333
[32] Bapir B, Abrahamczyk L, Wichtmann T, Prada-Sarmiento LF. Soil-structure interaction: a state-of-the-art review of modeling techniques and studies on seismic response of building structures. Front Built Environ. 2023 Feb;9:1120351. https://doi.org/10.3389/fbuil.2023.1120351
[33] Dhadse GD, Ramtekkar GD, Bhatt G. Finite element modeling of soil structure interaction system with interface: a review. Arch Comput Methods Eng. 2021 Aug;28(5):3415-32. https://doi.org/10.1007/s11831-020-09505-2
[34] Pandey G, Mourya VK, Patel D, Kumar R, Kumar S. Load sharing behaviour in piled-raft foundations over sand and clay: An experimental investigation. Res. Eng. Struct. Mater., 2024; 10(3): 917-942. http://dx.doi.org/10.17515/resm2023.41me0714rs
[35] Panji M, Mojtabazadeh-Hasanlouei S, Yasemi F. A half-plane time-domain BEM for SH-wave scattering by a subsurface inclusion. Comput Geosci. 2020 Jan;134:104342. https://doi.org/10.1016/j.cageo.2019.104342
[36] Panji M. A half-space TD-BEM model for a seismic corrugated orthotropic stratum. Eng Anal Bound Elem. 2023 Jul;152:655-77. https://doi.org/10.1016/j.enganabound.2023.04.032
[37] Mojtabazadeh-Hasanlouei S, Panji M, Kamalian M. Attenuated orthotropic time-domain half-space BEM for SH-wave scattering problems. Geophys J Int. 2022;229(3):1881-913. https://doi.org/10.1093/gji/ggac032
[38] Nienhuys H-W. Cutting in deformable objects [dissertation]. Utrecht (Netherlands): Utrecht University; 1975.
[39] Dhadse GD, Ramtekkar G, Bhatt G. Thin layer interface: An alternative modeling consideration in soil-structure interaction system. Res. Eng. Struct. Mater., 2024; 10(3): 1173- 1194. http://dx.doi.org/10.17515/resm2024.16me0926rs
[40] Messioud S, Dias D. Dynamic response of a rigid foundation rested in a densified soil. J Mater Eng Struct. 2023;10:19-32.
[41] Messioud S, Sbartai B, Dias D. Seismic response of a rigid foundation embedded in a viscoelastic soil by taking into account the soil-foundation interaction. Struct Eng Mech. 2016 Jun;58(5):887-903. https://doi.org/10.12989/sem.2016.58.5.887
[42] Benslama B, Bourahla N, Messioud S, Dias D. Vertical dynamic impedance for vibrations isolation of foundations using in-filled trenches. J GeoEng. 2023 Jun;18(2).

[43] Okyay US. Étude expérimentale et numérique des transferts de charge dans un massif renforcé par inclusions rigides: application à des cas de chargements statiques et dynamiques [dissertation]. Lyon: INSA; 2010.
[44] Messioud S, Okyay US, Sbartai B, Dias D. Dynamic response of pile reinforced soils and piled foundations. Geotech Geol Eng. 2016 Jun;34(3):789-805. https://doi.org/10.1007/s10706-016-0003-0
[45] Neghmouche Y, Messioud S, Dias D. Dynamic response of soil-piles-mattress-slab and soil-piles-slab systems under seismic loading. J GeoEng. 2022 Jun;17(2).
[46] Okyay US, Dias D, Billion P, Vandeputte D, Courtois A. Impedance functions of slab foundations with rigid piles. Geotech Geol Eng. 2012 Aug;30(4):1013-24. https://doi.org/10.1007/s10706-012-9523-4
[47] Antonutti R, Peyrard C, Incecik A, Ingram D, Johanning L. Dynamic mooring simulation with Code_Aster with application to a floating wind turbine. Ocean Eng. 2018 Mar;151:366-77. https://doi.org/10.1016/j.oceaneng.2017.11.018
[48] EDF Group. code_aster [Internet]. [cited 2025 Jun 4]. Available from: https://www.edf.fr/groupe-edf/inventer-l-avenir-de-l-energie/r-d-un-savoir-faire-mondial/nos-offres/codes-de-calcul/code-aster
[49] Delmas J. Stratégies de contrôle d'erreur en calcul de structures industrielles. Mise en oeuvre d'estimation d'erreur en quantité d'intérêt et d'adaptation de maillage [dissertation]. Amiens: Université de Picardie Jules Verne; 2008.
[50] Kudawoo AD. Problèmes industriels de grande dimension en mécanique numérique du contact: performance, fiabilité et robustesse [dissertation]. Marseille: Université de Provence - Aix-Marseille I; 2012.
[51] Geuzaine C, Remacle J. Gmsh: A 3-D finite element mesh generator with built-in pre- and post-processing facilities. Numer Methods Eng. 2009 Sep;79(11):1309-31. https://doi.org/10.1002/nme.2579
[52] Messioud S, Dias D, Sbartai B. Influence of the pile toe condition on the dynamic response of a group of pile foundations. Int J Adv Struct Eng. 2019 Mar;11(1):55-66. https://doi.org/10.1007/s40091-019-0217-5
[53] Kuhlemeyer RL, Lysmer J. Finite element method accuracy for wave propagation problems. J Soil Mech Found Div. 1973 May;99(5):421-7. https://doi.org/10.1061/JSFEAQ.0001885
[54] Grange S, Kotronis P, Mazars J. Modèle simplifié 3D de l'interaction sol structure: application au génie parasismique. In: 18ème Congrès Français de Mécanique; 2007 Aug; Grenoble, France.
[55] Do NA, Dias D, Oreste P. 2D seismic numerical analysis of segmental tunnel lining behaviour. Bull N Z Soc Earthq Eng. 2014 Sep;47(3):206-16. https://doi.org/10.5459/bnzsee.47.3.206-216
[56] Jiménez GAL, Dias D. Dynamic soil-structure interaction effects in buildings founded on vertical reinforcement elements. CivilEng. 2022 Jun;3(3):573-93. https://doi.org/10.3390/civileng3030034
[57] Messioud S, Dias D, Okyay US, Sbartai B. Impédances dynamiques de fondations sur groupe de pieux. In: XXIXe Rencontres Universitaires de Génie Civil; 2011 May 29-31; Tlemcen, Algeria.
[58] Padrón LA, Aznárez JJ, Maeso O. BEM-FEM coupling model for the dynamic analysis of piles and pile groups. Eng Anal Bound Elem. 2007 Jun;31(6):473-84. https://doi.org/10.1016/j.enganabound.2006.11.001
[59] Latini C, Zania V. Dynamic lateral response of suction caissons. Soil Dyn Earthq Eng. 2017 Sep;100:59-71. https://doi.org/10.1016/j.soildyn.2017.05.020
[60] Novak M, Nogami T. Soil-pile interaction in horizontal vibration. Earthq Eng Struct Dyn. 1977 Jul;5(3):263-81. https://doi.org/10.1002/eqe.4290050305
[61] Bouneguet S, Messioud S, Dias D. Vertical and horizontal dynamic response of suction caisson foundations. Stud Geotech Mech. 2023 Mar;45(1):1-13. https://doi.org/10.2478/sgem-2022-0018